NeuroImage: Clinical 32 (2021) 102867

Contents lists available at ScienceDirect

NeuroImage: Clinical

journal homepage: www.elsevier.com/locate/ynicl

Relayed nuclear Overhauser effect weighted (rNOEw) imaging identifies multiple sclerosis

Jianpan Huang [a,1], Jiadi Xu [b,c,1], Joseph H.C. Lai [a], Zilin Chen [a], Chi Yan Lee [d], Henry K.F. Mak [e], Koon Ho Chan [d,*], Kannie W.Y. Chan [a,c,f,g,*]

[a] Department of Biomedical Engineering, City University of Hong Kong, Hong Kong, China
[b] F.M. Kirby Research Center for Functional Brain Imaging, Kennedy Krieger Research Institute, Baltimore, MD, USA
[c] Russell H. Morgan Department of Radiology and Radiological Science, The Johns Hopkins University School of Medicine, Baltimore, MD, USA
[d] Department of Medicine, Li Ka Shing Faculty of Medicine, The University of Hong Kong, Pokfulam, Hong Kong, China
[e] Department of Diagnostic Radiology, Li Ka Shing Faculty of Medicine, The University of Hong Kong, Pokfulam, Hong Kong, China
[f] City University of Hong Kong Shenzhen Research Institute, Shenzhen, China
[g] Hong Kong Centre for Cerebro-Cardiovascular Health Engineering, Hong Kong, China

ARTICLE INFO

Keywords:
Magnetic resonance imaging (MRI)
Relayed nuclear Overhauser effect (rNOE)
Multiple sclerosis (MS)
Neuromyelitis optica spectrum disorders (NMOSD)
Myelin

ABSTRACT

Multiple sclerosis (MS) is an autoimmune disease of the central nervous system in which the immune system attacks the myelin and axons, consequently leading to demyelination and axonal injury. Magnetic resonance imaging (MRI) plays a pivotal role in the diagnosis of MS, and currently various types of MRI techniques have been used to detect the pathology of MS based on unique mechanisms. In this study, we applied the relayed nuclear Overhauser effect weighted (rNOEw) imaging to study human MS at clinical 3T. Three groups of subjects, including 20 normal control (NC) subjects, 14 neuromyelitis optica spectrum disorders (NMOSD) patients and 21 MS patients, were examined at a clinical 3T MRI scanner. Whole-brain rNOEw images of each subject were obtained by acquiring a control and a labeled image within four minutes. Significantly lower brain rNOEw contrast was detected in MS group compared to NC ($P = 0.008$) and NMOSD ($P = 0.014$) groups, while no significant difference was found between NC and NMOSD groups ($P = 0.939$). The lower rNOEw contrast of MS group compared to NC/NMOSD group was significant in white matter ($P = 0.041/0.021$), gray matter ($P = 0.004/0.020$) and brain parenchyma ($P = 0.015/0.021$). Moreover, MS lesions showed higher number and larger size but lower rNOEw contrast than NMOSD lesions ($P = 0.002$). Our proposed rNOEw imaging scheme has potential to serve as a new method for assisting MS diagnosis. Importantly, it may be used to identify MS from NMOSD.

1. Introduction

Multiple sclerosis (MS) is an autoimmune disease of the central nervous system (CNS) in which the immune system attacks the myelin (nerve fiber sheath) and axons, leading to demyelination and axonal injury. MS causes motor and cognitive impairments. Currently it affects more than two million people globally and is a major cause of disability in young adults (Browne et al., 2014; Sospedra and Martin, 2005; Thompson et al., 2018). Demyelination leads to the change of lipids and proteins in the brain, as dehydrated myelin consists of 75–80% lipids and 20–25% proteins by weight (Min et al., 2009). Currently most treatments aim at reducing inflammation to slow down the disease progression, while the efficacy could be very limited if patients are diagnosed at an advanced stage of the disease. Therefore, early diagnosis of MS is crucial to enhance treatment efficacy by starting effective disease modifying therapies early to avoid extensive demyelination and axonal injury (Thompson et al., 2018). Magnetic resonance imaging (MRI) plays a pivotal role in the early and accurate diagnosis of MS, enabling early interventions or treatments (Filippi et al., 2016). Many MRI techniques have been proposed to detect demyelination or relevant pathological changes in MS brain. Conventional methods, such as gadolinium (Gd)-enhanced T_1-weighted and T_2-weighted images, have been

* Corresponding authors at: City University of Hong Kong, 83 Tat Chee Avenue, Kowloon, Hong Kong, China (K.W.Y. Chan); The University of Hong Kong, 102 Pokfulam Road, Hong Kong, China (K.H. Chan).
E-mail addresses: koonho@hku.hk (K.H. Chan), KannieW.Y.C@cityu.edu.hk (K.W.Y. Chan).
[1] Authors contributed equally

https://doi.org/10.1016/j.nicl.2021.102867
Received 22 July 2021; Received in revised form 12 October 2021; Accepted 25 October 2021
Available online 28 October 2021

widely used to identify MS lesions with considerable sensitivity (Dalton et al., 2003; McDonald et al., 2001). Diffusion tensor imaging (DTI) or diffusional kurtosis imaging (DKI, which has the b value set to large value) has been used to quantify tissue properties, such as changes of water diffusion in myelin, which might not be visible using conventional MRI methods (Beaulieu, 2009; Gulani et al., 2001; Klawiter et al., 2011; Valsasina et al., 2005). Relaxometry methods, such as multicomponent T_2 mapping, can measure the myelin water fraction (MWF) by detecting short-T_2 water trapped between myelin layers. This enables the assessment of the myelin structure (Horch et al., 2011; Laule et al., 2006; Mackay et al., 1994). Magnetization transfer (MT) imaging is another MRI approach that detects the change of macromolecules, including myelin lipids/proteins, by applying a radiofrequency pulse at designated off-resonance frequency to selectively saturate bound pool of protons (Fernando et al., 2005; Schmierer et al., 2004). Previous studies have demonstrated the correlation between MTR and myelin content (Dousset et al., 1995; Dousset et al., 1992), showing large decreases of MTR in animal model with experimentally induced demyelination. A high correlation between macromolecular proton fraction and myelin content was also found in postmortem samples of MS patients using quantitative MT (qMT) (Schmierer et al., 2007). The inhomogeneous MT (ihMT) is a recently proposed MT technique, which detects the dipolar order of myelin sheaths with high sensitivity (Ercan et al., 2018; Manning et al., 2017; Varma et al., 2015a; Varma et al., 2015b). Other MRI techniques, such as ultrashort echo time (UTE) (Sheth et al., 2016) or zero echo time (ZTE) (Weiger et al., 2020), and quantitative susceptibility mapping (QSM) (Wisnieff et al., 2015) also showed potential to detect myelin change in MS brain.

Chemical exchange saturation transfer (CEST) MRI is a molecular imaging technique that can enhance the sensitivity of detecting low concentration proteins and metabolites through their natural exchangeable protons (Van Zijl and Yadav, 2011; Ward et al., 2000). Among endogenous CEST contrasts, relayed nuclear Overhauser effects (rNOE), attributed to mobile proteins and lipids, generate CEST contrasts at 0–5 ppm upfield from the water signal of the Z-spectrum (CEST spectrum) and have been applied in imaging diseases, such as Alzheimer's disease (AD) (Chen et al., 2019) and brain tumor (Goerke et al., 2019; Heo et al., 2016; Jones et al., 2013). rNOE imaging has high specificity towards mobile proteins and lipids and thus holds the potential to detect myelin change in MS brain, as myelin consists of abundant lipids and proteins (Baumann and Pham-Dinh, 2001). MT contrast and direct water saturation (DS) are two major contaminations in rNOE contrast especially at clinical field strengths (such as 3T) (Huang et al., 2021a; Xu et al., 2016). Recently, we developed a rNOE imaging scheme with MT suppression using an optimized pulsed-CEST sequence, i.e. variable delay multi-pulse (VDMP) sequence (Xu et al., 2014), to sensitively detect changes of mobile proteins and lipids in mouse brain at a preclinical 3T MRI scanner (Huang et al., 2021a; Xu et al., 2016). In addition to high sensitivity for detecting mobile proteins and lipids, this rNOE imaging scheme has the advantages of easy implementation and rapid postprocessing, making it readily to be translated to clinical MRI. Previous investigations have demonstrated the feasibility of using amide proton transfer weighted (APTw) imaging (Zhou et al., 2003) to detect myelin changes in MS (By et al., 2018; Lee et al., 2021; Sartoretti et al., 2019). Since the MTR asymmetry analysis was applied, changes detected in these studies included contributions from both amide protons and aliphatic protons (i.e. rNOE). Here, we applied our optimized rNOE imaging method to study the pathology changes regarding myelin lipids/proteins in MS patients by comparing with normal and neuromyelitis optica spectrum disorders (NMOSD) subjects at a clinical 3T MRI scanner.

2. Material and methods

2.1. Study subjects

All procedures were carried out in accordance with operational guidelines of Human Research Ethics Committee, and all protocols were approved by the local Institutional Review Board. Written informed consents to undergo MRI examination were obtained from subjects or relatives of patients who were unable to provide consents. Subjects were scanned at the MRI Center of The University of Hong Kong between July 2019 and March 2020. The subjects were composed of 20 normal control (NC) subjects, 14 patients with NMOSD and 21 patients with MS. Table 1 summarized gender distribution, mean age, age range and number of subjects. NMOSD were diagnosed according to the diagnostic criteria suggested by Wingerchuk et al. (Wingerchuk et al., 2006) in 2006 and conforming to the criteria updated in 2015 (Wingerchuk et al., 2015), while MS was diagnosed according to the 2010 revisions to the McDonald Criteria (Polman et al., 2011). The clinical diagnosis results, including the duration since clinical onset and the latest expanded disability status scale (EDSS), of NMOSD and MS patients were shown in Table 2.

2.2. MRI acquisition

All MRI scans were performed on a Philips 3T scanner (Achieva, Philips Healthcare, Best, The Netherlands) with a body coil for excitation and an eight-channel SENSitivity Encoding (SENSE) head coil for reception. Pulsed-CEST sequence was set up for rNOE imaging by modifying the turbo spin echo (TSE) sequence. The saturation parameters optimized in previous study on a preclinical 3T MRI scanner were applied here (Huang et al., 2021a). Briefly, the saturation module contained a pulse train with a saturation power (B_1) of 0.8 μT, a pulse duration (t_p) of 40 ms, a mixing time (t_{mix}) of 60 ms and a pulse number (N) of 10. Other MRI parameters were set as followings: repetition time (TR) = 3000 ms; echo time (TE) = 56 ms; flip angle (FA) = 90°; number of average (NA) = 1; Field of view (FOV) = 230 × 230 × 198 mm^3; acquisition matrix = 76 × 76 × 33; reconstruction matrix = 224 × 224 × 33; voxel size = 1.03 × 1.03 × 6 mm^3; SENSE factor = 2; scan time = 1 min 48 s. In this study, a control image set at −8 ppm and a labeled image set at −3.5 ppm were acquired, resulting in a total scan time of 3 min 36 s for each rNOEw image set. Fluid-attenuated inversion-recovery (FLAIR) images were also acquired as references. FLAIR parameters were set as followings: TR = 4800 ms; TE = 269 ms; inversion time (IT) = 1650 ms; FA = 90°; NA = 2; FOV = 250 × 250 × 198 mm^3; acquisition matrix = 208 × 208 × 330; reconstruction matrix = 512 × 512 × 330; voxel size = 0.49 × 0.49 × 0.6 mm^3; SENSE factor = 2; scan time = 4 min 34 s.

2.3. Data analysis

Image processing were performed using MATLAB (MathWorks, Natick, MA, USA) and FMRIB Software Library (FSL, https://fsl.fmrib.ox.ac.uk/fsl/fslwiki/FSL). The control image I_{con} and the labeled

Table 1
Demographic data of the study subjects.

	NC	NMOSD	MS
No. of subjects	20	14	21
Gender	18 Female and 2 Male	12 Female and 2 Male	17 Female and 4 Male
Age (year)	50 ± 12 (26–67) P = 0.500 (ns) to NMOSD	53 ± 11 (29–72) P = 0.006 (**) to MS	41 ± 12 (23–64) P = 0.022 (*) to NC

NC: normal control; NMOSD: neuromyelitis optica spectrum disorders; MS: multiple sclerosis; ns, not significant. Age data were presented as mean ± standard deviation (SD).

Table 2
Clinical diagnosis results of NMOSD and MS patients.

NMOSD			MS		
Subject No.	**Duration (year)**	**EDSS**	**Subject No.**	**Duration (year)**	**EDSS**
1	8	7	1	9	1
2	9	2	2	11	2
3	3	5.5	3	9	6.5
4	7	5.5	4	7	2
5	8	4	5	8	2
6	10	2	6	13	3
7	19	3	7	16	3
8	3	2	8	5	3
9	3	2	9	13	5.5
10	5	3	10	4	1
11	3	3	11	9	7
12	12	2	12	6	3
13	12	6	13	7	2.5
14	2	2	14	7	1
Mean ± SD	7.4 ± 4.8	3.5 ± 1.8	15	5	2
			16	8	1
			17	3	0.5
			18	7	1
			19	20	7
			20	4	1
			21	10	0.5
			Mean ± SD	8.6 ± 4.2	2.6 ± 2.1

Duration: duration since clinical onset; EDSS: expanded disability status scale (0–10). SD: standard deviation.

image I_{lab} were obtained for calculating the rNOE weighted (rNOEw) image using following equation:

$$rNOEw = \frac{I_{con} - I_{lab}}{I_{con}} \times 100\% \quad (1)$$

Here we used rNOEw signal to represent the observed rNOE signal as it might have minor contributions from residual DS/MT and T_1 relaxation. Brain region of each dataset was extracted from corresponding control image using BET in FSL and then segmented in to white matter and gray matter using FAST in FSL. Lesions were extracted with reference to FLAIR images. Volumes of brain and lesion were estimated by multiplying corresponding voxel number with the voxel size. After obtaining the rNOEw images, the mean values of rNOEw contrast from the whole brain and lesions were analyzed. GraphPad Prism 8 (GraphPad Software, San Diego, CA, USA) was used for statistical analysis. Unpaired student's *t* test was employed to evaluate the signal difference between diseases and control groups. Difference with P value of < 0.05 was regarded as significant. The receiver operating characteristic (ROC) analysis was used to assess the diagnostic performance of rNOEw contrast and Youden's index was used to identify the best cut-off value.

3. Results

An exemplary demonstration of rNOEw image calculation from a normal human brain using Eq. (1) was shown in Fig. 1. We can see that clear rNOEw images of the whole brain could be easily generated using control and labeled images acquired by the optimized pulsed-CEST MRI protocol. In the multi-slice rNOEw images, white matter showed hyperintensity, while gray matter showed hypointensity. This pattern was comparable with rNOE images generated using full Z-spectra in previous studies (Jones et al., 2013; Zaiss et al., 2015).

Representative brain rNOEw images, together with the average rNOEw contrasts of slices containing brain region, for NC, NMOSD and MS subjects were shown in Fig. 2. In general, the rNOEw images of NC brain were more homogeneous than the other two types of brain. Similar rNOEw contrasts were observed in NMOSD brain compared to NC brain (Fig. 2A, B). However, lower rNOEw contrast was observed in most slices of MS brain compared to NMOSD and NC brains (Fig. 2A–C), and these differences were found to be significant in most of slices (Fig. 2D). All P values of comparisons shown in Fig. 2D were given in Supplementary Table 1. The differences of rNOEw contrast between NC/NMOSD and MS were also confirmed with group comparison among three types of subjects (Fig. 3). The whole brain rNOEw contrast of MS group was significantly lower than that of NC group (7.30 ± 1.27% versus 8.52 ± 1.54%, P = 0.008) and NMOSD group (7.30 ± 1.27% vs. 8.56 ± 1.61%, P = 0.014). However, no significant difference was found between NC and NMOSD groups (P = 0.939). As the average age of MS group was younger than the other two groups (Table 1, P = 0.022 to NC and P = 0.006 to NMOSD), we further investigated if age could be a

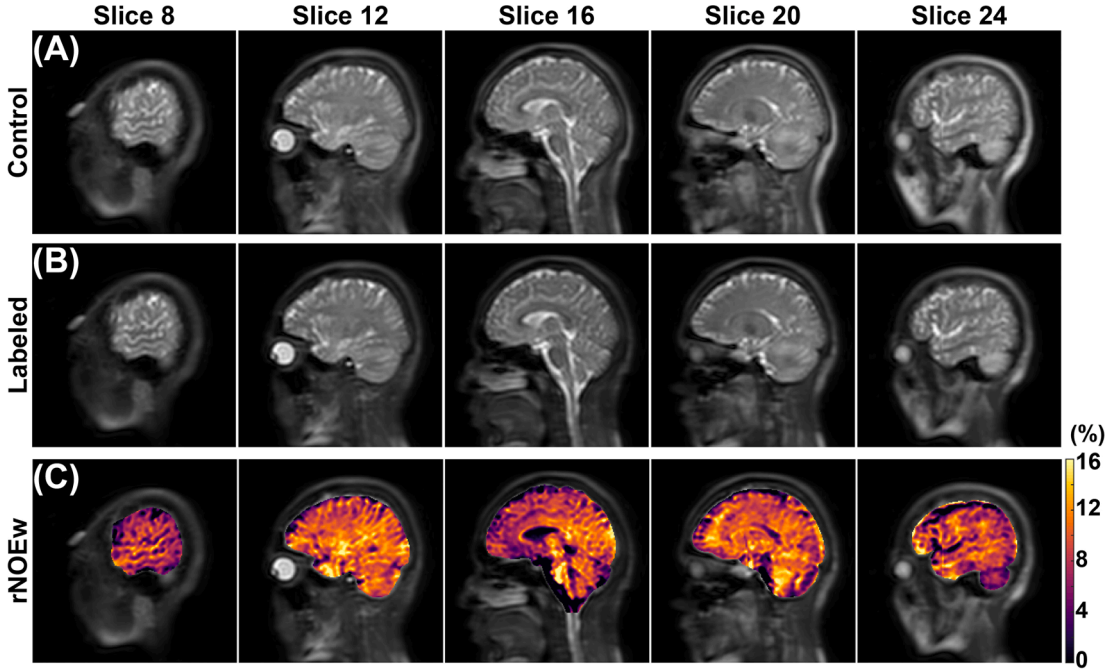

Fig. 1. An exemplary demonstration of generating (C) rNOE weighted (rNOEw) images using (A) control images and (B) labeled images.

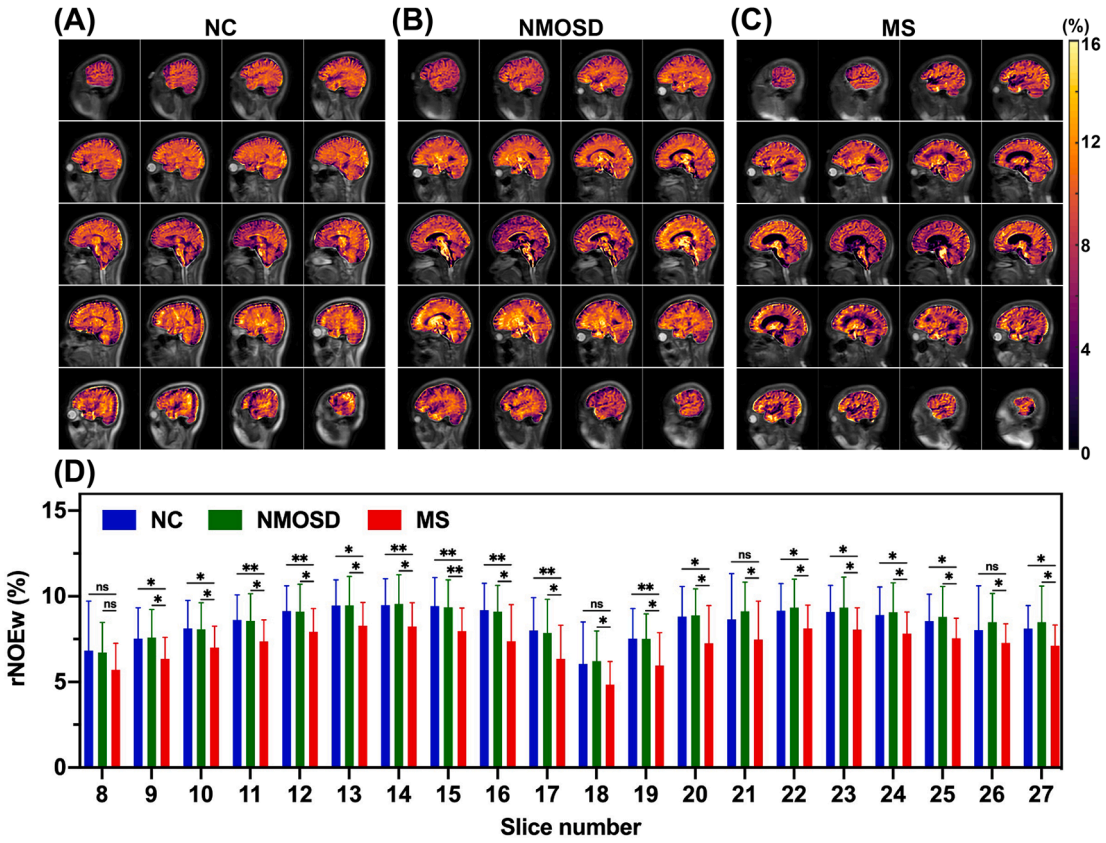

Fig. 2. Representative rNOEw images from central 20 brain slices (8–27) of (A) NC, (B) NMOSD and (C) MS. (D) Average rNOEw contrasts of all slices for NC (n = 20), NMOSD (n = 14) and MS (n = 21) groups. Significance levels: ns, not significant; *P < 0.05; **P < 0.01.

factor that influenced the comparison of rNOEw contrast. The MS patients were firstly sorted into age order and then divided into two groups (32 ± 5 years old and 51 ± 10 years old) with similar patient number (n = 11 and 10, respectively). As shown in Fig. 3B, no significant difference was observed between these two MS subgroups (P = 0.627). Interestingly, the decreased rNOEw contrast of MS groups than NC and NMOSD groups was also found to be significant in white matter (NC: P = 0.041; NMOSD: P = 0.021), gray matter (NC: P = 0.004; NMOSD: P = 0.020) and brain parenchyma, i.e. both white matter and gray matter (NC: P = 0.015; NMOSD: P = 0.021) (Fig. 3C–E). No significant difference of rNOEw contrast was found between NC and NMOSD groups in all three segmentations (white matter: P = 0.638; gray matter: P = 0.793; brain parenchyma: P = 0.838). We compared the volume of whole brain among three groups (NC: 1318 ± 141 cm^3; NMOSD: 1301 ± 131 cm^3; MS: 1316 ± 111 cm^3) but no significant difference was found (NC vs. MS: P = 0.971; NMOSD vs. MS: P = 0.715; NC vs. NMOSD: P = 0.731), as shown in Supplementary Fig. 1A. We further compared the volume of brain parenchyma (Supplementary Fig. 1B), as brain atrophy might appear inside the brain (Fig. 2C). Slight decrease of brain volume was found in MS group (1042 ± 129 cm^3) compared to NC group (1085 ± 115 cm^3) and NMOSD group (1066 ± 112 cm^3), but this did not reach significance (NC vs. MS: P = 0.265; NMOSD vs. MS: P = 0.567; NC vs. NMOSD: P = 0.639).

We further investigated the rNOEw contrast change in lesions of NMOSD and MS brains. For NMOSD, some (11 out of 14) patients were found with a few lesions in brain and most of lesions were in the form of small dot, as shown in Fig. 4A–C. However, massive lesions were observed in brain of all MS patients and the lesions (Fig. 4D–F) were much larger and more irregular than that of NMOSD patients. Since the lesions had different size, we calculated the average rNOEw contrast and volume of lesions for comparison between MS and NMOSD. Results showed that the rNOEw contrast of MS lesion was significantly lower (P = 0.002) than that of NMOSD (Fig. 5A), while lesion volume of MS was substantially larger (P = 0.002) than that of NMOSD (Fig. 5B). We also compared the rNOEw contrast between lesion (Fig. 5) and white matter (Fig. 3) where the lesions were detected (Fig. 4). As shown in Table 3, rNOEw contrast of NMOSD lesion was slightly lower than that of NC (P = 0.326) and NMOSD (P = 0.215) whiter matter and slightly higher than that of MS (P = 0.538) white matter, but these did not reach significance. However, rNOEw contrast of MS lesion was significantly lower than that of white matter of all three groups (P < 0.001). We then studied the correlation of the rNOEw contrast and volume of lesions with EDSS. Negative correlations were found between rNOEw contrast of lesion and EDSS (Fig. 6A & C), while positive correlations were observed between lesion volume and EDSS (Fig. 6B & D). The correlation levels were found to be significant in MS (P = 0.017 and P = 0.038 in Fig. 6C & D, respectively), but not in NMOSD (P = 0.154 and P = 0.622 in Fig. 6A & B, respectively).

We analyzed the ROC curves to investigate the performance of rNOEw imaging in MS diagnosis (Fig. 7). Results of whole brain showed that the MS patients could be identified from NC subjects with an area under curve (AUC) of 0.73, a sensitivity of 76.2% and a specificity of 70.0% at a cut-off rNOEw contrast of 7.92%, while they could be differentiated from NMOSD patients with an AUC of 0.72, a sensitivity of 81.0% and a specificity of 64.3% at a cut-off rNOEw contrast of 8.13% (Table 4). Similar results were found in the segmented brain regions. Notably, the NMOSD patients could not be identified from the NC subjects as all the AUC values were lower than 0.56 (Fig. 7C), which was consistent with the observation in Fig. 3.

4. Discussion

In this study, we applied our optimized rNOEw imaging technique for detecting MS pathology in the human brain at a clinical 3T MRI

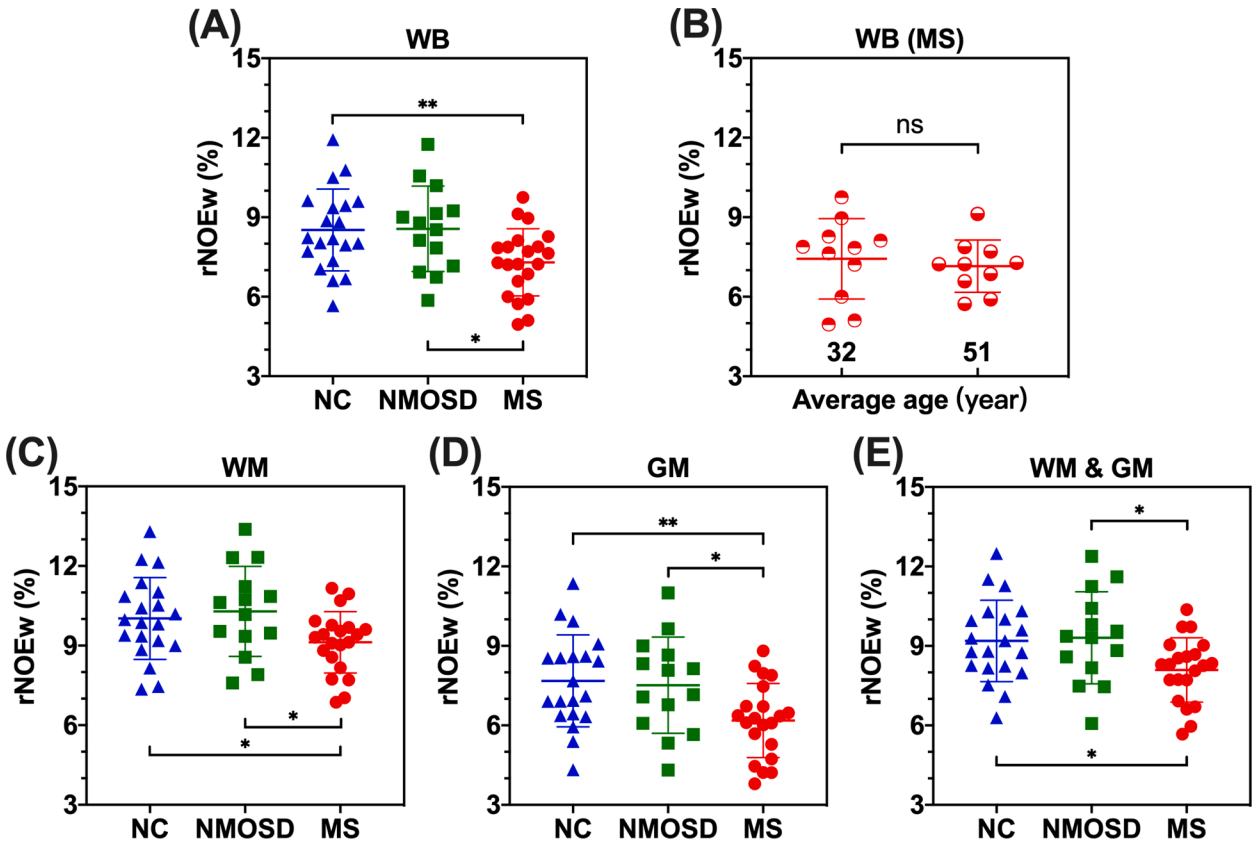

Fig. 3. The comparisons of average rNOEw contrast for NC (n = 20), NMOSD (n = 14) and MS (n = 21) groups. The rNOEw contrast comparisons of whole brain (WB) for (A) three groups and for (B) two MS subgroups with different ages (32-years old: n = 11; 51-years old: n = 10). The rNOEw contrast comparisons of (C) white matter (WM), (D) gray matter (GM) and (E) brain parenchyma (WM & GM) for three groups. Significance levels: ns, not significant; *P < 0.05; **P < 0.01.

scanner. Similar to most CEST studies, MT contrast and DS are two major contaminations in rNOE contrast. In previous animal study, we have developed and optimized a pulsed-CEST MRI scheme to rapidly obtain rNOEw images with MTC and DS suppression at a preclinical 3T scanner (Huang et al., 2021a). In this study, we applied the optimized pulsed-CEST scheme to obtain the rNOEw images from human brain by simply acquiring a labeled image I_{lab} at −3.5 ppm and a control image I_{con} at −8 ppm. Results showed that this scheme can quickly and robustly obtain good-quality rNOEw images covering the whole brain (Fig. 1) within 4 min, which indicated that it could be easily incorporated to the routine clinical examination without taking too much extra time. Hyperintensity in white matter and hypointensity in gray matter were detected, basically because myelin mostly localized within the white matter (Marner et al., 2003).

Here, rNOEw images from three types of human subjects, i.e. NC, NMOSD and MS, were acquired for comparison. An obvious lower rNOEw contrast was detected in brains of MS patients compared to the other two groups of subjects (Fig. 2). It is well known that myelin is necessary for healthy functioning of the CNS, and MS is one of inflammatory demyelinating diseases which have devastating effect on the cognitive and motor functions (Lucchinetti et al., 2000; Murray, 2006). Myelin is a sheath of multi-layered specialized membrane that is formed around axons in the CNS by oligodendrocytes. It is composed primarily of lipids along with a large variety of proteins (Jahn et al., 2009). Our rNOEw imaging scheme has been validated to have high sensitivity and specificity to monitor changes of the lipids/proteins (Huang et al., 2021a), thus being able to detect the lipids/proteins decrease induced by the demyelination in MS brains (Fig. 3). This study has demonstrated that our proposed rNOEw imaging scheme can be used to facilitate MS diagnosis, nevertheless, further study is underway to explore the specific contributions to the rNOEw contrast changes during the disease progress. MS has been conventionally regarded as a white matter disease, but demyelination has also been found in gray matter of chronic MS (Bo et al., 2006; Bø et al., 2003; Geurts and Barkhof, 2008). Here, substantially decreased rNOEw contrast of MS than NC was not only found in white matter (P = 0.041) but also in gray matter (P = 0.004), indicating that gray matter might also suffer from demyelination in these MS patients. The onset age of MS is typically young, as some studies report an average age at onset lower than 30 years old (Cierny et al., 2017; Ligouri et al., 2000). This could be a reason that the average age of MS group was younger than the NC and NMOSD groups (Table 1). Nevertheless, the age difference was not contributing to the decreased in rNOEw contrast of MS in this study, since no significant difference of rNOEw contrast was found between 32-years old and 51-years old MS subgroups (Fig. 3B).

NMOSD is sometimes misdiagnosed as MS especially at the early stage, as the presenting neurological features are similar. These include acute transverse myelitis and optic neuritis. However, the CNS pathologies are different in NMOSD and MS, suggesting different mechanisms of brain injury (Kawachi and Lassmann, 2017; Pittock and Lucchinetti, 2016). In NMOSD, the water channel aquaporin-4 is the target of the pathogenic autoantibodies presenting in the serum of the majority of NMOSD patients, and binding of aquaporin-4 autoantibodies to CNS aquaporin-4 is believed to trigger neuroinflammation via both complement-dependent and complement-independent mechanisms with secondary demyelination, axonal and neuronal injuries (Yick et al., 2018). In contrast, migration of activated lymphocytes from peripheral blood into the CNS is believed to trigger inflammatory demyelination and axonal injury in MS (Sospedra and Martin, 2005; Thompson et al., 2018). Thus, conventional diffusion imaging could have limitations in identifying these neuropathologies. In this study, the EDSS were found to be similar in NMOSD and MS groups (3.5 ± 1.8 versus 2.6 ± 2.1),

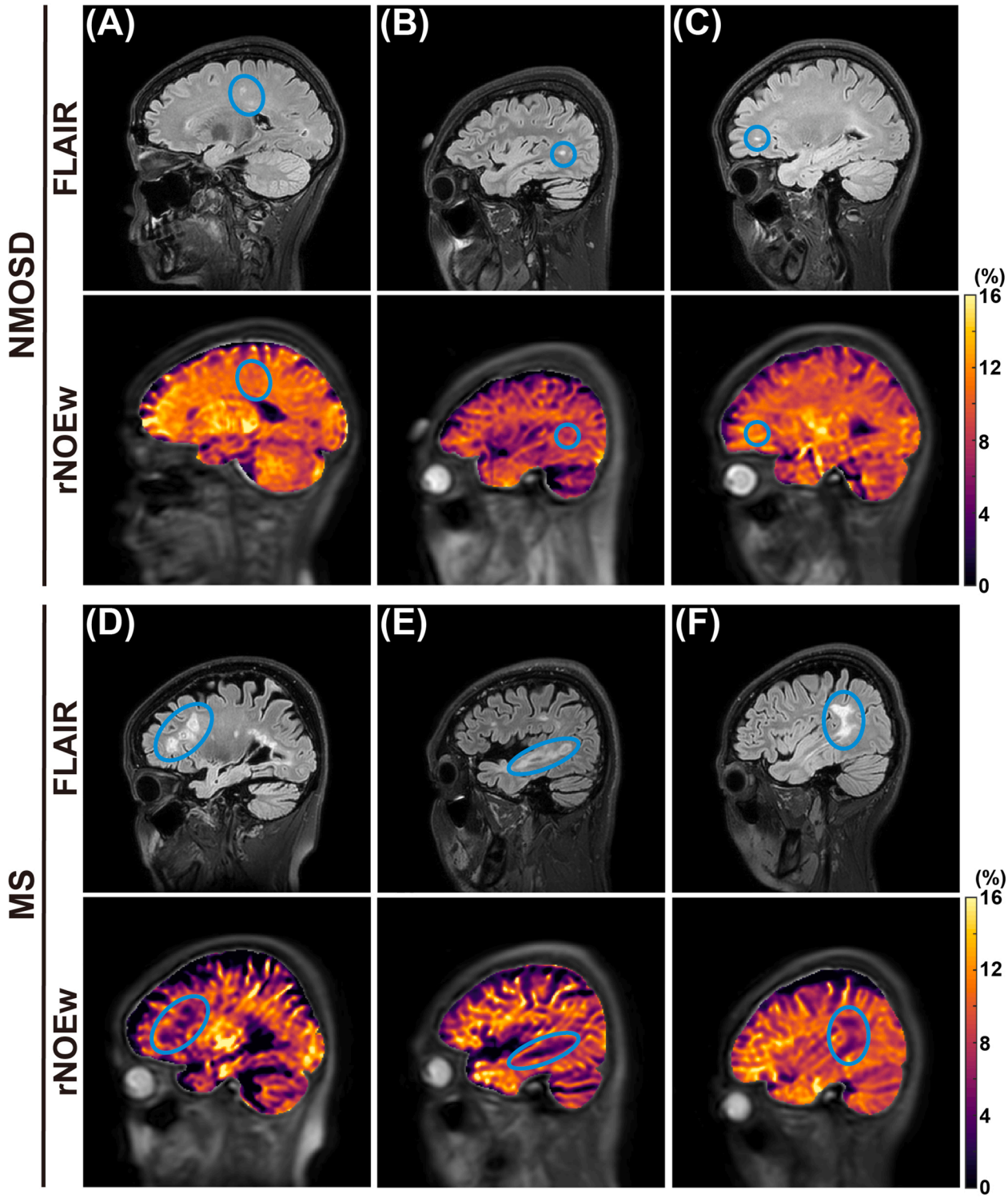

Fig. 4. Representative lesion-containing rNOEw images, together with corresponding fluid-attenuated inversion-recovery (FLAIR) images, of (A-C) three NMOSD patients and (D-F) three MS patients. Lesions were circumscribed by blue. (For interpretation of the references to colour in this figure legend, the reader is referred to the web version of this article.)

indicating a minor difference of disability status between these two groups. However, we found that rNOEw imaging could sensitively differentiate MS from NMOSD, as significant lower rNOEw contrast was found in the MS group compared to NMOSD group ($P = 0.014$). Moreover, substantial differences were also found in white matter ($P = 0.021$) and gray matter ($P = 0.020$). Therefore, rNOEw imaging has potential for identifying MS from NMOSD, which could be attributed to the specificity of rNOEw imaging towards myelin lipids/protein. The rNOEw results showed that the number and size of MS lesions were much larger than that of NMOSD lesions (Figs. 4 & 5B). Besides, NMOSD lesions showed comparable rNOEw contrast with surrounding white matter, whereas the MS lesion showed substantially lower rNOEw contrast than white matter of all three groups (Table 3). Therefore, the rNOEw contrast of MS lesion was significantly lower than that of

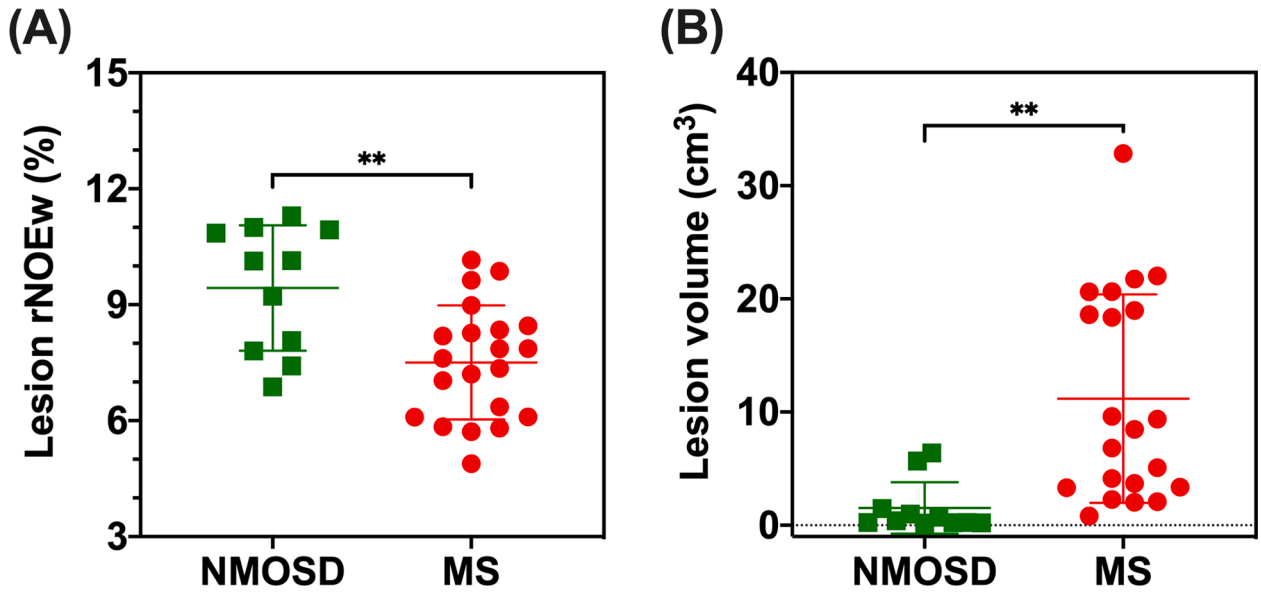

Fig. 5. Lesion comparison between NMOSD (n = 11, excluding three patients without lesion) and MS (n = 21) groups. (A) Comparison of lesion rNOEw contrast. (B) Comparison of lesion volume. Significance levels: **P < 0.01.

Table 3
Comparison of rNOEw contrast between lesion and white matter (WM).

	NC WM 10.02 ± 1.54%	NMOSD WM 10.29 ± 1.70%	MS WM 9.12 ± 1.16%
NMOSD Lesion 9.43 ± 1.62%	P = 0.326 (ns)	P = 0.215 (ns)	P = 0.538 (ns)
MS Lesion 7.51 ± 1.68%	P < 0.001 (***)	P < 0.001 (***)	P < 0.001 (***)

The number under each group name indicated the mean and standard deviation of rNOEw contrast of corresponding group. ns, not significant.

NMOSD (Fig. 5A). The lesion results strongly supported the different neuropathology in these two diseases, where similar observations were also reported by previous studies (Matthews et al., 2013; Sinnecker et al., 2012). Obviously decreased rNOEw contrast was found in MS lesions compared to surrounding normal brain region (Fig. 4D–F), indicating that rNOEw imaging was sensitive to myelin lipids/protein related changes. Interestingly, the correlations of EDSS with rNOEw contrast and volume of lesions were significant in MS (Fig. 6C & D), indicating that the disability status of MS patients was largely attributed to lesion load (Fisniku et al., 2008). Similar correlation trends were observed in NMOSD group but not significant, which needed more validation in the future as the patient number of NMOSD was less than MS in current study.

In rNOE or other CEST studies, saturation parameters need to be specifically optimized according to the static field strength (B_0). At low field strengths, the saturation power has to be low enough to avoid large DS effect. Owing to the extremely slow exchange rate (≤20 Hz), rNOE can be fully saturated even with low saturation powers (<1 μT) (Huang et al., 2021a; Huang et al., 2021b). This makes rNOE imaging suitable for clinical applications at 3T. To further investigate the influence of DS contamination under different field strengths, the simulations based on Bloch-McConnell equations including three pools (DS, MT and rNOE) were performed using the same saturation parameters with this study. Other simulation parameters were approximately assigned with reference to previous studies, (Chen et al., 2019; Huang et al., 2021a; Jin and Kim, 2021; Khlebnikov et al., 2017; Rooney et al., 2007), as listed in Supplementary Table 2. From the simulation results (Fig. S3), the DS effect at −3.5 ppm was negligible under 3T (0.69%) and 7T (0.24%) compared to the corresponding rNOEw contrast (8.32% and 10.09%, respectively). However, this imaging method became challenged at 1.5T, as the DS effect contributed to a large portion of the calculated rNOEw contrast (2.14% out of 6.64%). In this case, the full Z-spectra need to be acquired to exclude the DS effect using Lorentzian fitting, which would result in longer scan time.

The rNOEw imaging technique requires two scans for control and labeled images, thus motion issue needs to be considered. To assess the degree of motion in this study, we calculated the structural similarity index (SSIM) (Wang et al., 2004) between control and labeled images for all investigated subjects. Notably, the SSIM used here only included the structural term but not the intensity-related terms as the control and labeled images by nature had different image intensity due to the different saturation offsets. We found that the motion level was negligible in current study as the SSIM values of all subjects were higher than 0.995, as shown in Supplementary Fig. 3. For representative rNOEw images with different average rNOEw contrasts, the SSIM maps were homogeneous with values close to 1 (Supplementary Fig. 3A). Moreover, no correlation was found between average rNOEw contrasts and SSIM values for all investigated subjects (Supplementary Fig. 3B). Therefore, the motion correction should not be critical in this study.

There were some limitations in this study when we primarily considered the total scan time to be <5 min in this pilot study: (i) The voxel size especially in the sagittal dimension (6 mm thickness) was too large. Thus, brain structures and NMOSD/MS lesions were blurred in rNOEw images. In the future study, the acquisition module of rNOE imaging sequence needs to be optimized to achieve high spatial resolution and reasonable temporal resolution. (ii) B_1 map was not acquired. Previous study reported that B_1 correction improved the CEST image quality and provided clear glioma rim (Windschuh et al., 2015). It is highly recommended to collect B_1 map for correction of rNOE image in the future investigation, which could benefit the identification of MS lesion. As for B_0 issue, the rNOE signal is insensitive to a drift of <0.5 ppm at 3 T due to its broad peak (Huang et al., 2021a). If the scanner has large B_0 inhomogeneity, water saturation shift referencing (WASSR) (Kim et al., 2009) could be included in the acquisition protocol for post-correction. (iii) T_1 relaxation could contribute to the observed rNOE/CEST signals, this was one reason that we used rNOEw contrast to represent the observed rNOE contrast in this study. The level of influence depends on the T_1 difference between lesion and normal tissue. One possible solution is to acquire the T_1 map and then calculate the apparent exchange-dependent relaxation (AREX) to reveal the chemical

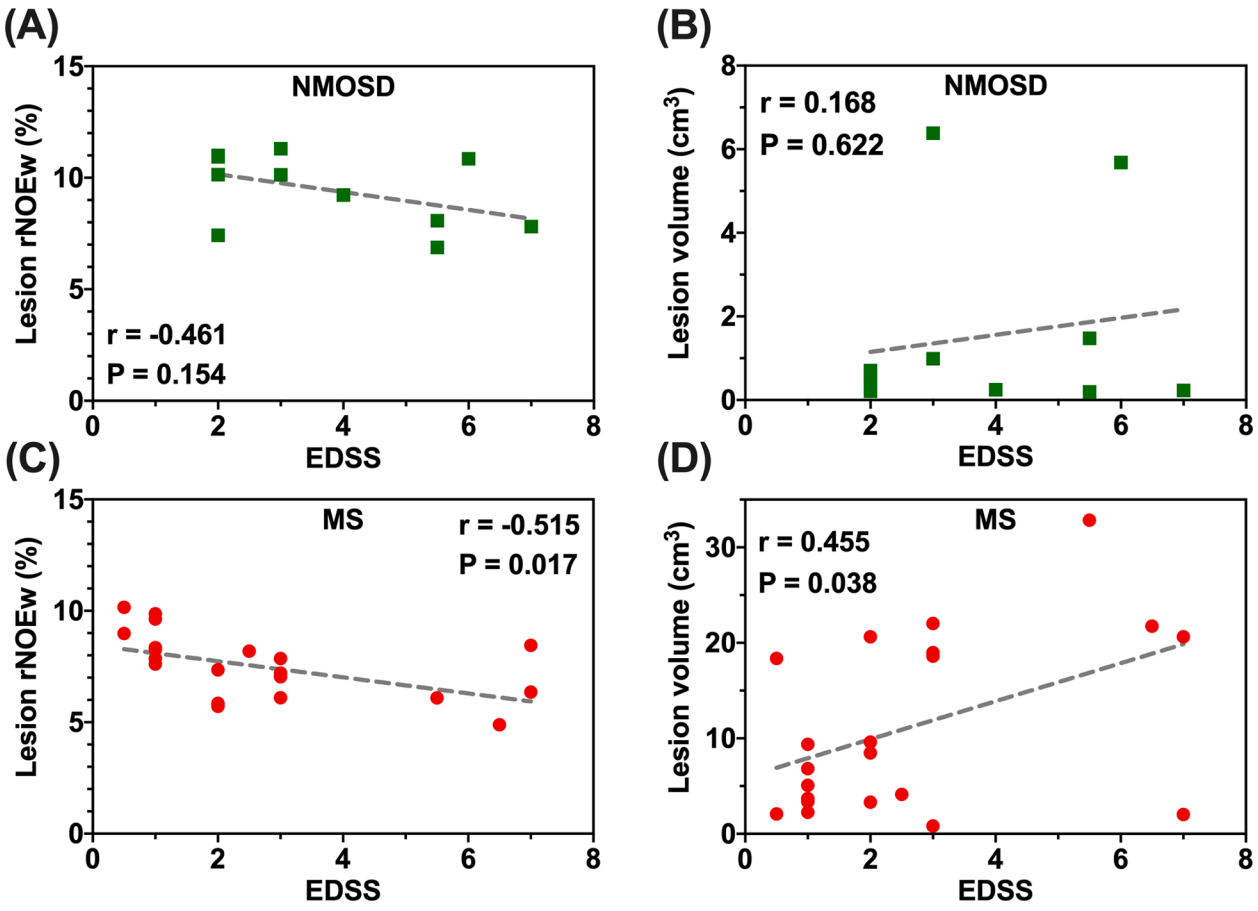

Fig. 6. Correlation results between EDSS and (A&C) rNOEw contrast /(B&D) volume of lesions, for (A&B) NMOSD and (C&D) MS groups.

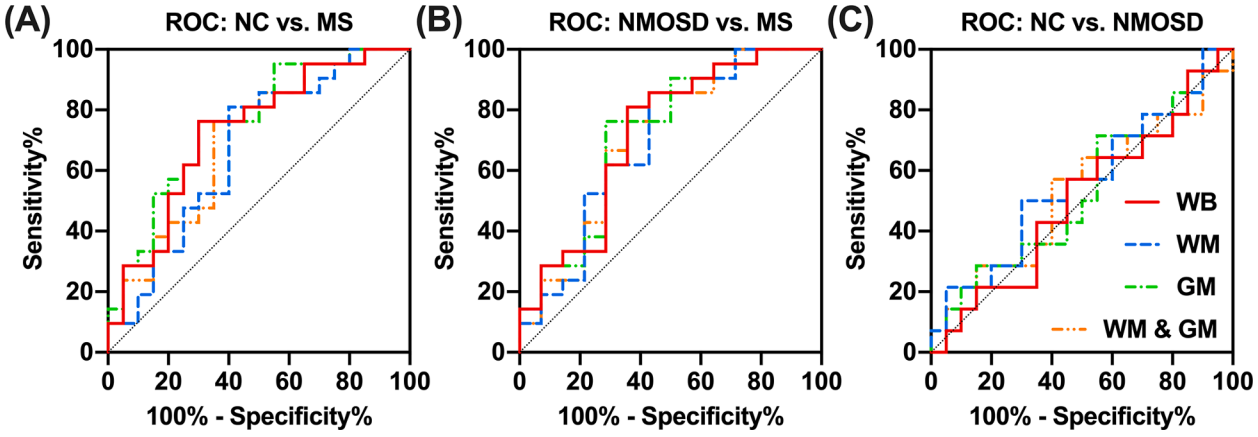

Fig. 7. Receiver operating characteristic (ROC) analysis of rNOEw contrast as an imaging biomarker for diagnosis of MS. ROC analysis between (A) NC and MS, (B) NMOSD and MS, and (C) NC and NMOSD (NC: n = 20; NMOSD: n = 14; MS: n = 21).

exchange-related effect (Zaiss et al., 2015), but this might not be necessary for cases with small T_1 variation. Various MRI techniques have been applied in MS diagnosis currently, the origin of signal changes upon demyelination or remyelination could be different. For example, DTI/DKI detect the myelin structure, relaxation methods (such as MWF) measure the myelin water changes, while MTR methods detect the information of all macromolecules. We speculated that rNOEw imaging could provide supplementary information regarding the myelin lipids/proteins. Therefore, multiparametric study incorporating other MRI techniques can be performed in the future for a comprehensive assessment of related neuropathology in MS. Besides, longitudinal studies could be useful for exploring the rNOE signal changes related to the MS disease progression. Nevertheless, as a proof-of-concept study, our results have already demonstrated that rNOEw imaging has potential for assisting MS diagnosis.

5. Conclusions

In this study, we applied our optimized pulsed-CEST MRI scheme for rapid rNOEw imaging (<4 min) to investigate the pathology changes related to myelin lipids/proteins in MS at a clinical 3T scanner. No substantial difference of rNOEw contrast was detected in NMOSD group

Table 4
Performance of rNOEw contrast for MS diagnosis estimated based on receiver operating characteristic (ROC) analysis.

	Region	AUC (95% CI)	Sensitivity (95% CI) (%)	Specificity (95% CI) (%)	Cut-off value (%)
NC vs. *MS*	*WB*	0.73 (0.57–0.89)	76.2 (54.9–89.4)	70.0 (48.1–85.5)	7.92
	WM	0.67 (0.51–0.84)	81.0 (60.0–92.3)	60.0 (38.7–78.1)	9.79
	GM	0.75 (0.61–0.90)	76.2 (54.9–89.4)	70.0 (48.1–85.5)	6.81
	WM & GM	0.70 (0.53–0.86)	76.2 (54.9–89.4)	65.0 (43.3–81.9)	8.71
NMOSD vs. *MS*	*WB*	0.72 (0.54–0.90)	81.0 (60.0–92.3)	64.3 (38.8–83.7)	8.13
	WM	0.70 (0.51–0.89)	85.7 (65.4–95.0)	57.1 (32.6–78.6)	10.04
	GM	0.72 (0.54–0.90)	76.2 (54.9–89.4)	71.4 (45.4–88.3)	6.75
	WM & GM	0.71 (0.52–0.90)	76.2 (54.9–89.4)	64.3 (38.8–83.7)	8.75

AUC, area under the ROC curve; CI, confidence interval; WB: whole brain; WM: white matter; GM: gray matter; The cut-off value was determined by Youden's index.

compared to NC group, while significantly lower rNOEw contrast was found in MS group compared to above two groups. Notably, an obvious decrease of rNOEw contrast was observed in MS lesion region compared to normal-appearing brain tissue, indicating the sensitivity of rNOEw imaging towards myelin changes. Our proposed rNOEw imaging scheme has potential to serve as a new way for assisting MS diagnosis, importantly it holds promise to identify MS from NMOSD.

6. Grant Support

Research Grants Council: 11102218, PDFS2122-1S01; City University of Hong Kong: 7005210, 9667198, 7005433, 7005626 and 9609307; National Natural Science Foundation of China: 81871409; Food and Health Bureau of Hong Kong Government (Health and Medical Research Fund: 05160086).

CRediT authorship contribution statement

Jianpan Huang: Conceptualization, Methodology, Investigation, Formal analysis, Writing – original draft, Visualization. **Jiadi Xu:** Conceptualization, Methodology, Investigation, Formal analysis, Writing – review & editing. **Joseph H.C. Lai:** Investigation, Formal analysis. **Zilin Chen:** Investigation, Formal analysis. **Chi Yan Lee:** Investigation. **Henry K.F. Mak:** Investigation, Formal analysis, Writing – review & editing. **Koon Ho Chan:** Investigation, Formal analysis, Writing – review & editing, Funding acquisition. **Kannie W.Y. Chan:** Conceptualization, Methodology, Investigation, Formal analysis, Writing – review & editing, Funding acquisition, Supervision, Project administration.

Declaration of Competing Interest

KWYC, JX, and JH are listed on a related patent application. All other authors declare no conflict of interest.

Acknowledgements

Authors thank Mr. Joseph Siu-Tong Tse from Department of Diagnostic Radiology, The University of Hong Kong for assisting with the MRI acquisition. We are grateful to receive funding support from the Research Grants Council: 11102218, PDFS2122-1S01; City University of Hong Kong: 7005210, 9667198, 7005433, 7005626 and 9609307; National Natural Science Foundation of China: 81871409; Food and Health Bureau of Hong Kong Government (Health and Medical Research Fund: 05160086).

Appendix A. Supplementary data

Supplementary data to this article can be found online at https://doi.org/10.1016/j.nicl.2021.102867.

References

Baumann, N., Pham-Dinh, D., 2001. Biology of oligodendrocyte and myelin in the mammalian central nervous system. Physiol. Rev. 81 (2), 871–927.
Beaulieu, C., 2009. Diffusion MRI: from quantitative measurement to in vivo neuroanatomy (Johansen-Berg H, Behrens TEJ, eds). Elsevier, London.
Bo, L., Geurts, J.J.G., Mork, S.J., Valk, P., 2006. Grey matter pathology in multiple sclerosis. Acta Neurol. Scand. 113 (s183), 48–50.
Bø, L., Vedeler, C.A., Nyland, H.I., Trapp, B.D., Mørk, S.J., 2003. Subpial demyelination in the cerebral cortex of multiple sclerosis patients. J. Neuropathol. Exp. Neurol. 62 (7), 723–732.
Browne, P., Chandraratna, D., Angood, C., Tremlett, H., Baker, C., Taylor, B.V., Thompson, A.J., 2014. Atlas of multiple sclerosis 2013: a growing global problem with widespread inequity. Neurology 83 (11), 1022–1024.
By, S., Barry, R.L., Smith, A.K., Lyttle, B.D., Box, B.A., Bagnato, F.R., Pawate, S., Smith, S. A., 2018. Amide proton transfer CEST of the cervical spinal cord in multiple sclerosis patients at 3T. Magn. Reson. Med. 79 (2), 806–814.
Chen, L., Wei, Z., Chan, K.W.Y., Cai, S., Liu, G., Lu, H., Wong, P.C., van Zijl, P.C.M., Li, T., Xu, J., 2019. Protein aggregation linked to Alzheimer's disease revealed by saturation transfer MRI. Neuroimage 188, 380–390.
Cierny, D., Lehotsky, J., Hanysova, S., Michalik, J., Kantorova, E., Sivak, S., Kurca, E., Dobrota, D., Jesenska, L., 2017. The age at onset in Multiple Sclerosis is associated with patient's prognosis. Bratisl. Lek. Listy 118 (06), 374–377.
Dalton, C.M., Brex, P.A., Miszkiel, K.A., Fernando, K., MacManus, D.G., Plant, G.T., Thompson, A.J., Miller, D.H., 2003. New T2 lesions enable an earlier diagnosis of multiple sclerosis in clinically isolated syndromes. Ann. Neurol. 53 (5), 673–676.
Dousset, V., Brochet, B., Vital, A., Gross, C., Benazzouz, A., Boullerne, A., Bidabe, A.-M., Gin, A.-M., Caille, J.-M., 1995. Lysolecithin-induced demyelination in primates: preliminary in vivo study with MR and magnetization transfer. Am. J. Neuroradiol. 16, 225–231.
Dousset, V., Grossman, R.I., Ramer, K.N., Schnall, M.D., Young, L.H., Gonzalez-Scarano, F., Lavi, E., Cohen, J.A., 1992. Experimental allergic encephalomyelitis and multiple sclerosis: lesion characterization with magnetization transfer imaging. Radiology 182 (2), 483–491.
Ercan, E., Varma, G., Mädler, B., Dimitrov, I.E., Pinho, M.C., Xi, Y., Wagner, B.C., Davenport, E.M., Maldjian, J.A., Alsop, D.C., Lenkinski, R.E., Vinogradov, E., 2018. Microstructural correlates of 3D steady-state inhomogeneous magnetization transfer (ihMT) in the human brain white matter assessed by myelin water imaging and diffusion tensor imaging. Magn. Reson. Med. 80 (6), 2402–2414.
Fernando, K., Tozer, D., Miszkiel, K., Gordon, R., Swanton, J., Dalton, C., Barker, G., Plant, G., Thompson, A., Miller, D., 2005. Magnetization transfer histograms in clinically isolated syndromes suggestive of multiple sclerosis. Brain 128, 2911–2925.
Filippi, M., Rocca, M.A., Ciccarelli, O., De Stefano, N., Evangelou, N., Kappos, L., Rovira, A., Sastre-Garriga, J., Tintorè, M., Frederiksen, J.L., Gasperini, C., Palace, J., Reich, D.S., Banwell, B., Montalban, X., Barkhof, F., 2016. MRI criteria for the diagnosis of multiple sclerosis: MAGNIMS consensus guidelines. Lancet Neurol. 15 (3), 292–303.
Fisniku, L.K., Brex, P.A., Altmann, D.R., Miszkiel, K.A., Benton, C.E., Lanyon, R., Thompson, A.J., Miller, D.H., 2008. Disability and T2 MRI lesions: a 20-year follow-up of patients with relapse onset of multiple sclerosis. Brain 131 (3), 808–817.
Geurts, J.JG., Barkhof, F., 2008. Grey matter pathology in multiple sclerosis. Lancet Neurol. 7 (9), 841–851.
Goerke, S., Soehngen, Y., Deshmane, A., Zaiss, M., Breitling, J., Boyd, P.S., Herz, K., Zimmermann, F., Klika, K.D., Schlemmer, H.-P., Paech, D., Ladd, M.E., Bachert, P., 2019. Relaxation-compensated APT and rNOE CEST-MRI of human brain tumors at 3 T. Magn. Reson. Med. 82 (2), 622–632.
Gulani, V., Webb, A.G., Duncan, I.D., Lauterbur, P.C., 2001. Apparent diffusion tensor measurements in myelin-deficient rat spinal cords. Magn. Reson. Med. 45 (2), 191–195.
Heo, H.-Y., Zhang, Y.i., Lee, D.-H., Hong, X., Zhou, J., 2016. Quantitative assessment of amide proton transfer (APT) and nuclear Overhauser enhancement (NOE) imaging with extrapolated semi-solid magnetization transfer reference (EMR) signals: Application to a rat glioma model at 4.7 tesla. Magn. Reson. Med. 75 (1), 137–149.
Horch, R.A., Gore, J.C., Does, M.D., 2011. Origins of the ultrashort-T2 1H NMR signals in myelinated nerve: a direct measure of myelin content? Magn. Reson. Med. 66 (1), 24–31.
Huang, J., Han, X., Chen, L., Xu, X., Xu, J., Chan, K.W.Y., 2021a. Relayed nuclear Overhauser enhancement imaging with magnetization transfer contrast suppression at 3 T. Magn. Reson. Med. 85 (1), 254–267.
Huang, J., Lai, J.H., Tse, K.-H., Cheng, G.W., Liu, Y., Chen, Z., Han, X., Chen, L., Xu, J., Chan, K.W., 2021b. Deep neural network based CEST and AREX processing: Application in imaging a model of Alzheimer's disease at 3 T. Magn. Reson. Med. https://doi.org/10.1002/mrm.29044.

Jahn, O., Tenzer, S., Werner, H.B., 2009. Myelin proteomics: molecular anatomy of an insulating sheath. Mol. Neurobiol. 40 (1), 55–72.
Jin, T., Kim, S.G., 2021. Role of chemical exchange on the relayed nuclear Overhauser enhancement signal in saturation transfer MRI. Magn. Reson. Med. https://doi.org/10.1002/mrm.28961.
Jones, C.K., Huang, A., Xu, J., Edden, R.A.E., Schär, M., Hua, J., Oskolkov, N., Zacà, D., Zhou, J., McMahon, M.T., Pillai, J.J., van Zijl, P.C.M., 2013. Nuclear Overhauser enhancement (NOE) imaging in the human brain at 7 T. Neuroimage 77, 114–124.
Kawachi, I., Lassmann, H., 2017. Neurodegeneration in multiple sclerosis and neuromyelitis optica. J. Neurol. Neurosurg. Psychiatry 88 (2), 137–145.
Khlebnikov, V., Windschuh, J., Siero, J.C., Zaiss, M., Luijten, P.R., Klomp, D.W., Hoogduin, H., 2017. On the transmit field inhomogeneity correction of relaxation-compensated amide and NOE CEST effects at 7 T. NMR Biomed. 30, e3687.
Kim, M., Gillen, J., Landman, B.A., Zhou, J., van Zijl, P.C.M., 2009. Water saturation shift referencing (WASSR) for chemical exchange saturation transfer (CEST) experiments. Magn. Reson. Med. 61 (6), 1441–1450.
Klawiter, E.C., Schmidt, R.E., Trinkaus, K., Liang, H.-F., Budde, M.D., Naismith, R.T., Song, S.-K., Cross, A.H., Benzinger, T.L., 2011. Radial diffusivity predicts demyelination in ex vivo multiple sclerosis spinal cords. Neuroimage 55 (4), 1454–1460.
Laule, C., Leung, E., Li, D.KB., Traboulsee, A.L., Paty, D.W., MacKay, A.L., Moore, G.RW., 2006. Myelin water imaging in multiple sclerosis: quantitative correlations with histopathology. Mult. Scler. J. 12 (6), 747–753.
Lee, D.-W., Heo, H., Woo, D.-C., Kim, J.K., Lee, D.-H., 2021. Amide proton transfer-weighted 7-T MRI contrast of myelination after cuprizone administration. Radiology 299 (2), 428–434.
Ligouri, M., Pugliatti, M., Giuliani, F., Robertis, F.D., Zimatore, G.B., Livrea, P., Trojano, M., Cocco, E., Marrosu, M.G., 2000. Age at onset in multiple sclerosis. Neurol. Sci. 21 (0), S825–S829.
Lucchinetti, C., Bruck, W., Parisi, J., Scheithauer, B., Rodriguez, M., Lassmann, H., 2000. Heterogeneity of multiple sclerosis lesions: implications for the pathogenesis of demyelination. Ann. Neurol. Official J. Am. Neurol. Assoc. Child Neurol. Soc. 47 (6), 707–717.
Mackay, A., Whittall, K., Adler, J., Li, D., Paty, D., Graeb, D., 1994. In vivo visualization of myelin water in brain by magnetic resonance. Magn. Reson. Med. 31 (6), 673–677.
Manning, A.P., Chang, K.L., MacKay, A.L., Michal, C.A., 2017. The physical mechanism of "inhomogeneous" magnetization transfer MRI. J. Magn. Reson. 274, 125–136.
Marner, L., Nyengaard, J.R., Tang, Y., Pakkenberg, B., 2003. Marked loss of myelinated nerve fibers in the human brain with age. J. Comparative Neurol. 462 (2), 144–152.
Matthews, L., Marasco, R., Jenkinson, M., Kuker, W., Luppe, S., Leite, M.I., Giorgio, A., De Stefano, N., Robertson, N., Johansen-Berg, H., Evangelou, N., Palace, J., 2013. Distinction of seropositive NMO spectrum disorder and MS brain lesion distribution. Neurology 80 (14), 1330–1337.
McDonald, W.I., Compston, A., Edan, G., Goodkin, D., Hartung, H.-P., Lublin, F.D., McFarland, H.F., Paty, D.W., Polman, C.H., Reingold, S.C., Sandberg-Wollheim, M., Sibley, W., Thompson, A., Van Den Noort, S., Weinshenker, B.Y., Wolinsky, J.S., 2001. Recommended diagnostic criteria for multiple sclerosis: guidelines from the International Panel on the diagnosis of multiple sclerosis. Ann. Neurol. 50 (1), 121–127.
Min, Y., Kristiansen, K., Boggs, J.M., Husted, C., Zasadzinski, J.A., Israelachvili, J., 2009. Interaction forces and adhesion of supported myelin lipid bilayers modulated by myelin basic protein. Proc. Natl. Acad. Sci. 106 (9), 3154–3159.
Murray, T.J., 2006. Diagnosis and treatment of multiple sclerosis. BMJ 332 (7540), 525–527.
Pittock, S.J., Lucchinetti, C.F., 2016. Neuromyelitis optica and the evolving spectrum of autoimmune aquaporin-4 channelopathies: a decade later. Ann. N. Y. Acad. Sci. 1366, 20.
Polman, C.H., Reingold, S.C., Banwell, B., Clanet, M., Cohen, J.A., Filippi, M., Fujihara, K., Havrdova, E., Hutchinson, M., Kappos, L., Lublin, F.D., Montalban, X., O'Connor, P., Sandberg-Wollheim, M., Thompson, A.J., Waubant, E., Weinshenker, B., Wolinsky, J.S., 2011. Diagnostic criteria for multiple sclerosis: 2010 revisions to the McDonald criteria. Ann. Neurol. 69 (2), 292–302.
Rooney, W.D., Johnson, G., Li, X., Cohen, E.R., Kim, S.-G., Ugurbil, K., Springer, C.S., 2007. Magnetic field and tissue dependencies of human brain longitudinal 1H2O relaxation in vivo. Magn. Reson. Med. 57 (2), 308–318.
Sartoretti, E., Sartoretti, T., Wyss, M., Becker, A.S., Schwenk, Á., van Smoorenburg, L., Najafi, A., Binkert, C., Thoeny, H.C., Zhou, J., Jiang, S., Graf, N., Czell, D., Sartoretti-Schefer, S., Reischauer, C., 2019. Amide proton transfer weighted imaging shows differences in multiple sclerosis lesions and white matter hyperintensities of presumed vascular origin. Front. Neurol. 10 https://doi.org/10.3389/fneur.2019.01307.
Schmierer, K., Scaravilli, F., Altmann, D.R., Barker, G.J., Miller, D.H., 2004. Magnetization transfer ratio and myelin in postmortem multiple sclerosis brain. Ann. Neurol. 56 (3), 407–415.
Schmierer, K., Tozer, D.J., Scaravilli, F., Altmann, D.R., Barker, G.J., Tofts, P.S., Miller, D.H., 2007. Quantitative magnetization transfer imaging in postmortem multiple sclerosis brain. J. Magn. Reson. Imaging 26 (1), 41–51.
Sheth, V., Shao, H., Chen, J., Vandenberg, S., Corey-Bloom, J., Bydder, G.M., Du, J., 2016. Magnetic resonance imaging of myelin using ultrashort Echo time (UTE) pulse sequences: Phantom, specimen, volunteer and multiple sclerosis patient studies. Neuroimage 136, 37–44.
Sinnecker, T., Dorr, J., Pfueller, C.F., Harms, L., Ruprecht, K., Jarius, S., Bruck, W., Niendorf, T., Wuerfel, J., Paul, F., 2012. Distinct lesion morphology at 7-T MRI differentiates neuromyelitis optica from multiple sclerosis. Neurology 79 (7), 708–714.
Sospedra, M., Martin, R., 2005. Immunology of multiple sclerosis. Annu. Rev. Immunol. 23 (1), 683–747.
Thompson, A.J., Baranzini, S.E., Geurts, J., Hemmer, B., Ciccarelli, O., 2018. Multiple sclerosis. Lancet 391 (10130), 1622–1636.
Valsasina, P., Rocca, M.A., Agosta, F., Benedetti, B., Horsfield, M.A., Gallo, A., Rovaris, M., Comi, G., Filippi, M., 2005. Mean diffusivity and fractional anisotropy histogram analysis of the cervical cord in MS patients. Neuroimage 26 (3), 822–828.
van Zijl, P.C.M., Yadav, N.N., 2011. Chemical exchange saturation transfer (CEST): what is in a name and what isn't? Magn. Reson. Med. 65 (4), 927–948.
Varma, G., Duhamel, G., de Bazelaire, C., Alsop, D.C., 2015a. Magnetization transfer from inhomogeneously broadened lines: a potential marker for myelin. Magn. Reson. Med. 73 (2), 614–622.
Varma, G., Girard, O.M., Prevost, V.H., Grant, A.K., Duhamel, G., Alsop, D.C., 2015b. Interpretation of magnetization transfer from inhomogeneously broadened lines (ihMT) in tissues as a dipolar order effect within motion restricted molecules. J. Magn. Reson. 260, 67–76.
Wang, Z., Bovik, A.C., Sheikh, H.R., Simoncelli, E.P., 2004. Image quality assessment: from error visibility to structural similarity. IEEE Trans. Image Process. 13 (4), 600–612.
Ward, K.M., Aletras, A.H., Balaban, R.S., 2000. A new class of contrast agents for MRI based on proton chemical exchange dependent saturation transfer (CEST). J. Magn. Reson. 143 (1), 79–87.
Weiger, M., Froidevaux, R., Baadsvik, E.L., Brunner, D.O., Rösler, M.B., Pruessmann, K.P., 2020. Advances in MRI of the myelin bilayer. Neuroimage 217, 116888. https://doi.org/10.1016/j.neuroimage.2020.116888.
Windschuh, J., Zaiss, M., Meissner, J.E., Paech, D., Radbruch, A., Ladd, M.E., Bachert, P., 2015. Correction of B1-inhomogeneities for relaxation-compensated CEST imaging at 7 T. NMR Biomed. 28, 529–537.
Wingerchuk, D.M., Banwell, B., Bennett, J.L., Cabre, P., Carroll, W., Chitnis, T., de Seze, J., Fujihara, K., Greenberg, B., Jacob, A., Jarius, S., Lana-Peixoto, M., Levy, M., Simon, J.H., Tenembaum, S., Traboulsee, A.L., Waters, P., Wellik, K.E., Weinshenker, B.G., 2015. International consensus diagnostic criteria for neuromyelitis optica spectrum disorders. Neurology 85 (2), 177–189.
Wingerchuk, D.M., Lennon, V.A., Pittock, S.J., Lucchinetti, C.F., Weinshenker, B.G., 2006. Revised diagnostic criteria for neuromyelitis optica. Neurology 66 (10), 1485–1489.
Wisnieff, C., Ramanan, S., Olesik, J., Gauthier, S., Wang, Y.i., Pitt, D., 2015. Quantitative susceptibility mapping (QSM) of white matter multiple sclerosis lesions: interpreting positive susceptibility and the presence of iron. Magn. Reson. Med. 74 (2), 564–570.
Xu, J., Yadav, N.N., Bar-Shir, A., Jones, C.K., Chan, K.W.Y., Zhang, J., Walczak, P., McMahon, M.T., van Zijl, P.C.M., 2014. Variable delay multi-pulse train for fast chemical exchange saturation transfer and relayed-nuclear overhauser enhancement MRI. Magn. Reson. Med. 71 (5), 1798–1812.
Xu, X., Yadav, N.N., Zeng, H., Jones, C.K., Zhou, J., van Zijl, P.C.M., Xu, J., 2016. Magnetization transfer contrast–suppressed imaging of amide proton transfer and relayed nuclear overhauser enhancement chemical exchange saturation transfer effects in the human brain at 7T. Magn. Reson. Med. 75 (1), 88–96.
Yick, L.-W., Ma, O.-F., Ng, R.-L., Kwan, J.-C., Chan, K.-H., 2018. Aquaporin-4 autoantibodies from neuromyelitis optica spectrum disorder patients induce complement-independent immunopathologies in mice. Front. Immunol. 9 https://doi.org/10.3389/fimmu.2018.01438.
Zaiss, M., Windschuh, J., Paech, D., Meissner, J.-E., Burth, S., Schmitt, B., Kickingereder, P., Wiestler, B., Wick, W., Bendszus, M., Schlemmer, H.-P., Ladd, M.E., Bachert, P., Radbruch, A., 2015. Relaxation-compensated CEST-MRI of the human brain at 7 T: unbiased insight into NOE and amide signal changes in human glioblastoma. Neuroimage 112, 180–188.
Zhou, J., Payen, J.-F., Wilson, D.A., Traystman, R.J., van Zijl, P.C.M., 2003. Using the amide proton signals of intracellular proteins and peptides to detect pH effects in MRI. Nat. Med. 9 (8), 1085–1090.